Journal of Imaging Informatics in Medicine (2025) 39:1666–1674
https://doi.org/10.1007/s10278-025-01611-6

Development and Evaluation of an Automated Histomorphometric Analysis Method for the Assessment of Implant Osseointegration

Lucas de Sousa Goulart Pereira[1] · Jovânia Alves Oliveira[1] · Elcio Marcantonio Jr[2] · André Ricardo Backes[3] · Guilherme José Pimentel Lopes de Oliveira[1]

Received: 15 January 2025 / Revised: 3 July 2025 / Accepted: 7 July 2025 / Published online: 28 July 2025

Abstract

This study evaluated an automated histomorphometric analysis method for assessing implant osseointegration. Sixty-eight histological images of implants installed in the tibiae of 40 rats were analyzed using the manual method and ImageJ software to evaluate the %BIC (bone-implant contact) and %BBT (bone between the implant threads). In the automated histomorphometric analysis method, the similarity of the RGB color channels was analyzed, and the black background region of the image was excluded, to select the region of interest. The contour curve was extracted, excluding points that do not belong to the contact between the implant and the bone, i.e., the image edges. A Gaussian filter was applied to smooth small imperfections in the curve. An analysis of the curve points in relation to their neighboring points was conducted, and the local maximum of the curve was selected, excluding points that were too close together and keeping only those that represent the peaks of the implant curve. The peaks and the corresponding portion of the curve were used to select the region of the original image and calculate the %BIC and %BBT values. A comparison of the results obtained for both parameters in both evaluation methods was then performed using Pearson's correlation test. A strong correlation was observed between the analyses ($r = 0.99$). Thus, the proposed automated histomorphometric analysis method was shown to be reliable for assessing implant osseointegration.

Keywords Osseointegration · Histomorphometry · Automated analysis · Computational vision

Introduction

The assessment of osseointegration of titanium implants is a widely used analysis to evaluate the interaction of the implants surface and bone tissue that is a key factor to indicate the quality of these devices [1]. In Dentistry, dental implants are an important option for the rehabilitation of patients who have lost one or multiple teeth, impairing masticatory function, phonetics, and social interaction due to aesthetic deficiencies [2, 3]. Due to the popularization of oral rehabilitation with implants, numerous experimental studies have been conducted aiming to improve the osseointegration process to improve the predictability of this phenomenon in a myriad of clinical conditions [4–7].

Osseointegration depends on the characteristics of the implants, especially their macrostructure and microstructure. The development of new implant designs and the need for testing under more challenging biological conditions make it necessary to evaluate these phenomena through histomorphometric analyses [4, 8, 9]. For the evaluation of implant osseointegration in experimental or clinical studies, the bone-implant contact (BIC) and amount of bone between the threads of the implant (BBT) are analyzed using histological slides obtained from collected samples [6, 10]. Indeed, these parameters indicate the relationship between the implants surfaces and the bone tissue of the host resulting in the fixation of the dental implants that enables resistance to support the occlusal load promoted by the prosthesis. BIC and BBT

✉ André Ricardo Backes
arbackes@yahoo.com.br

✉ Guilherme José Pimentel Lopes de Oliveira
guilherme.lopesoliveira@ufu.br

[1] Department of Periodontology, School of Dentistry, Universidade Federal de Uberlândia-UFU, Pará, Av., 1760-1844, Umuarama, Uberlândia, MG 38405-320, Brazil

[2] Department of Diagnosis and Surgery, Araraquara School of Dentistry, Univ Est Paulista (FOAr-UNESP), Araraquara, São Paulo, Brazil

[3] Department of Computing, Center for Exact Sciences and Technology, Federal University of São Carlos–UFSCar, Rod, Washington LuizSão Carlos, SP 13565-905, Brazil

are parameters related to how connected the implant is to the bone tissue, thus, higher values of BIC and BBT mean the implant is more connected to the bone tissue. This type of method is also useful to determine the biological potential of implants surfaces in the obtention of the osseointegration in different types of bone and in distinct systemic conditions. This information is important in the indication of different dental implants in the treatment of different types of edentulism. So, the BIC and BBT analysis are of great importance to provide these outcomes that guided clinical decision-making. This evaluation is performed manually with the help of software for image analysis, a complex process that requires significant training and work time [4, 11, 12]. In addition, the evaluator must be trained to reduce the error analysis that is common to occur in non-experienced evaluators.

With recent technological advancements, studies have been conducted to evaluate the performance of automated histological analysis processes, in order to streamline the process and improve the quality of the analyses, reducing the possibility of human errors [13, 14]. In medicine, the term "computational pathology" has been used to refer to an interdisciplinary science that promotes the development of computational approaches to analyze and model medical histopathology images [15]. The use of computational methods has been adopted to assist medical sciences in various ways: in the segmentation of nuclei and white blood cell counting [16, 17], detection and segmentation of nuclei in gastric cancer images [18], histological slide color correction using artificial intelligence [19, 20], and clinical applications of artificial intelligence in the identification of cancers and other oral pathologies [21, 22].

Due to the advantages of automation in the process of evaluating histological images, the development of these methods is necessary to reduce the evaluation time and improve accuracy when assessing the osseointegration process. The objective of this premilinary study was to develop and evaluate a script based on computer vision capable of automating the analysis of implant osseointegration through BIC and BBT values of implants installed in the tibiae of rats in order to speed up and improve the process of obtaining BIC and BBT values.

Methods

This study was previously approved by the Animal Ethics Committee of the Federal University of Uberlândia (UFU), protocol no. 030/20. For this study, 48 rats (Rattus norvegicus, Wistar strain) aged 3 months, weighing between 250 and 300 g, were kept in an environment with controlled temperature (21 ± 1 °C), humidity (65–70%), and light cycles (12 h). The animals were fed with appropriate food and had access to water and food ad libitum. This study was conducted according to the ARRIVE guidelines for conducting preclinical studies.

Sample Collection and Histological Slide Preparation

The 68 histological images evaluated in this study were manufactured for a previous study (Process CEUA/FOAr #32/2016). The animals were kept in an environment with controlled temperature (21 ± 1 °C), humidity (65–70%), and light cycles (12 h), fed with appropriate food and had access to water and food ad libitum. The study was conducted according to the ARRIVE guidelines for conducting preclinical studies. In that study, the animals were subjected to treatment with supra-physiological doses of testosterone, and the effect of this treatment on the osseointegration of implants with untreated surfaces was evaluated. A total of 40 animals were used. After 14- and 42-days post-implant placement, the animals were euthanized, and two tibiae with the implants were collected and fixed in 4% paraformaldehyde for 48 h.

The samples were then dehydrated in a graded series of ethanol (60–100%) and infiltrated with a light-curing resin (Technovit 7200 VLC, Kultzer Heraus GmbH & CO, Wehrheim, Germany). The blocks containing the implant and bone tissue were sectioned at a central point using a grinding system (Exakt Apparatebeau, Hamburg, Germany), obtaining two cuts per tibia. The final sections were approximately 45 µm thick and stained with Stevenel's blue associated with acidic fuchsine before being analyzed under an optical microscope (DIASTAR products-Leica Reichert & Jung, Wetzlar, Germany) with a 100 × magnification. Histomorphometric analyses were performed using image analysis software (ImageJ, San Rafael, CA, USA). The percentage of bone-implant contact (%BIC) and the bone area between the threads (%BBT) were analyzed in the first six threads of the implants (approximately 1.25 mm in length). These analyses were performed by a blinded and trained examiner.

Manual Analysis of %BIC and %BBT

Using a tracing tool, the total length of the implant surface was determined, followed by the length of the bone tissue in contact with the implant surface, allowing obtention of the percentage of bone in contact with the implant (%BIC). Using the same tracing tool, the total area between the threads of the implant was determined, followed by the total area of bone tissue between the threads of the implant, which enabled us to obtain the percentage of bone tissue between the threads of the implant (%BBT) (Fig. 1).

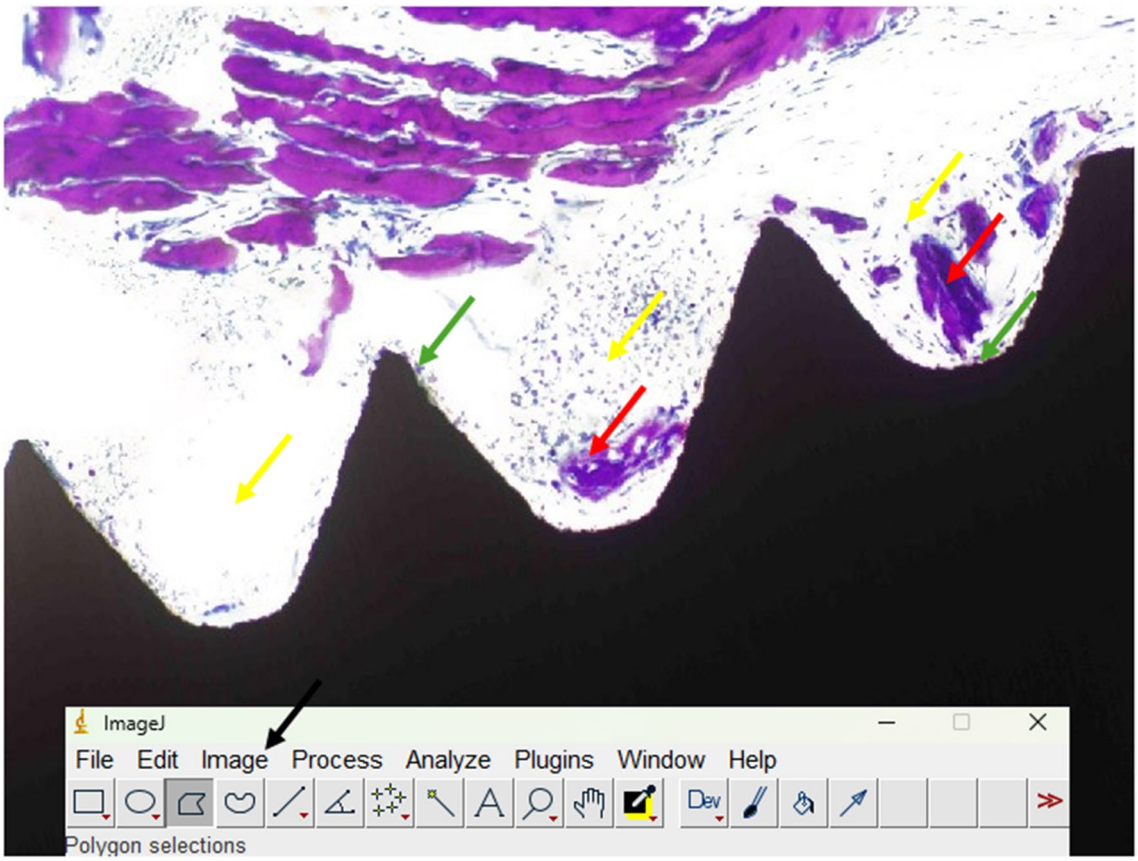

Fig. 1 Image representing manual analysis of BIC and BBT. Black arrow, indicates the toolbar of the ImageJ; Green arrow, indicates the contact of bone tissue to implant surface (BIC); Red arrow, indicates the area of bone tissue between the threads of the implant (BBT); Yellow arrow, indicates the area between the threads of the implant

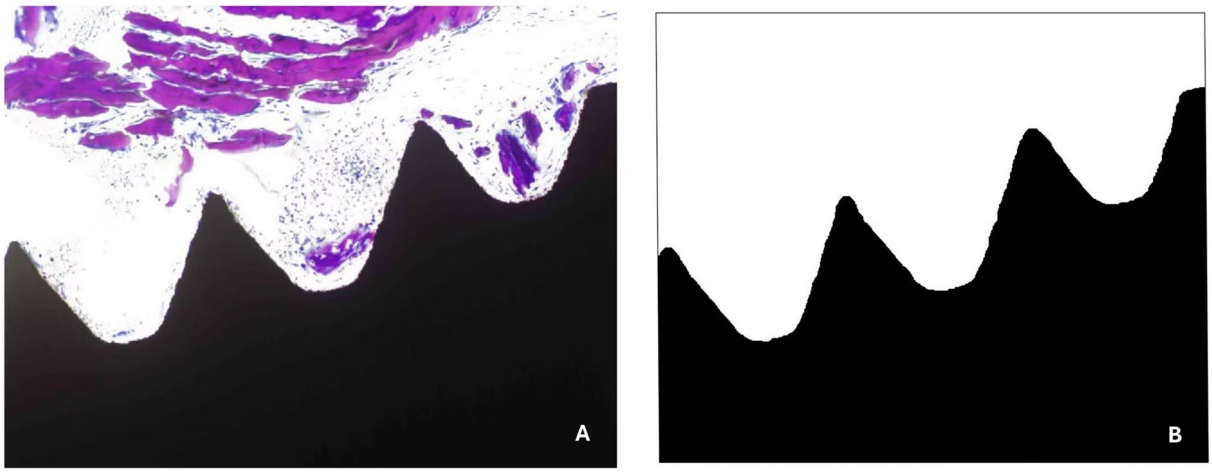

Fig. 2 **A** Image after spatial orientation. **B** Image after applying the filter that separates the region of implant from the bone region

Preprocessing

First, we pre-processed the images to ensure that they were all oriented in the same way, that is, with the region of the implant, identified by the black color in the images, at the bottom of the image (Fig. 2A). This step is necessary to ensure standardization and facilitate the subsequent analysis steps.

Segmentation

The segmentation step aims to separate the implant region from the bone region of the image. To accomplish this, we computed (i) the average of the image's RGB channels, μ_{RGB}, and (ii) the average of the difference between each pair of RGB channels, $diff_{RGB}$. We selected the image region with $\mu_{RGB} < 100$ and $diff_{RGB} < 40$ as the implant region. In the complementary region (bone), we applied a closing operation using a disc of $r = 15$ as a structuring element to correct imperfections in the segmentation. We then defined the implant region as the largest connected component in the image. The final step removes small points and other artifacts left from previous segmentation steps, thus resulting in the segmented image S (Fig. 2B).

Contour Extraction

Given the segmented image S, we extracted the contour, i.e., the set of ordered points that represents the limits of the object (Fig. 3A). We removed points that coincide with the edges of the image, i.e., large sequences of points having the same values on the X- or Y-axes. This resulted in the contour region that represents the contact between the bone and the implant, C. As the segmentation process can generate small flaws and noise in the contour, smoothing is necessary (Fig. 3B). We applied Fourier transform to the contour spectrum combined with a Gaussian of $\sigma = 13$ to smooth the contour. For this step, we also used a process of replicating and repeating the curve to preserve its extremities [23].

Region of Interest (ROI) Detection

The contour region that represents the contact area between the bone and implant presents a zigzag pattern defined by the implant thread. Therefore, to calculate the BIC and BBT, it is necessary to detect the various peaks formed by the implant thread. This is done by analyzing each point on the contour with its two neighbors (anterior and posterior), located at a distance $d = 15$. A point with value on the Y-axis that is greater than its two neighbors is considered a probable peak (Fig. 4A). As the segmentation process generates imperfections, some points may be erroneously detected as false peaks. Thus, we applied a filtering process to select only the four most relevant peaks, i.e., those equally distant from each other, as the points necessary for the BIC and BBT calculation (Fig. 4B).

Detection of BIC and BBT Regions

We selected the contour segment from the first to the last peak of the implant thread and then dilated this region in the segmented image S using a disc with radius $r = 3$ as a structuring element. This was performed to increase the area analyzed and provide greater confidence in the result. This region represents the set of points used to compute the BIC (Fig. 5A). We also selected the region delimited by the peaks and this contour segment, which defines the area to be analyzed by BBT (Fig. 5B).

Computing BIC and BBT

After defining the regions, it is necessary to separate the different elements of the original image to correctly compute the BIC and BBT (Fig. 6). These elements are represented

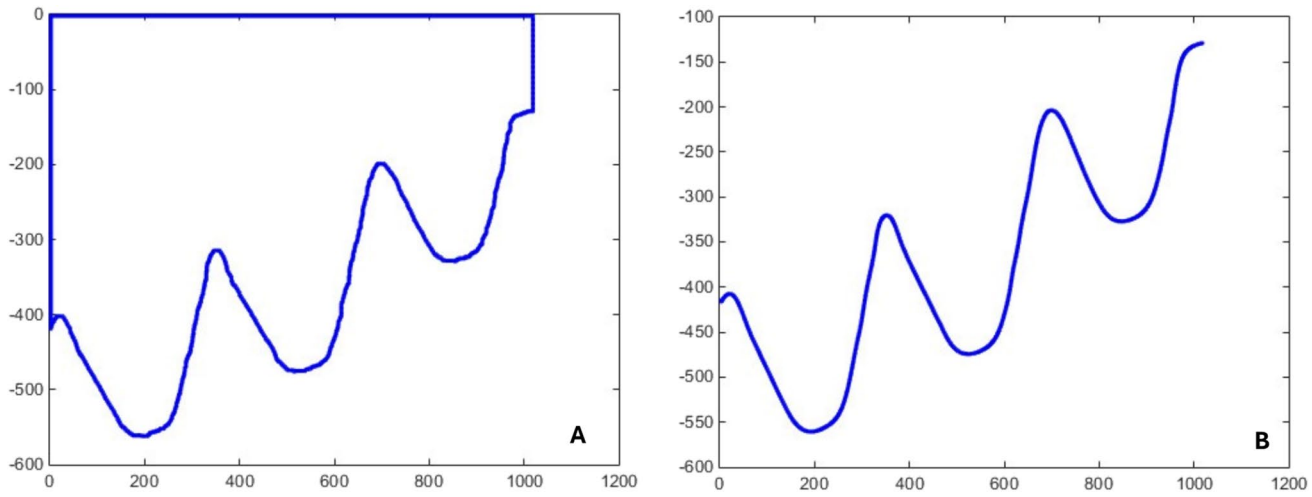

Fig. 3 **A** The area contour extracted from segmented image. **B** Contour of the implant surface after smoothing

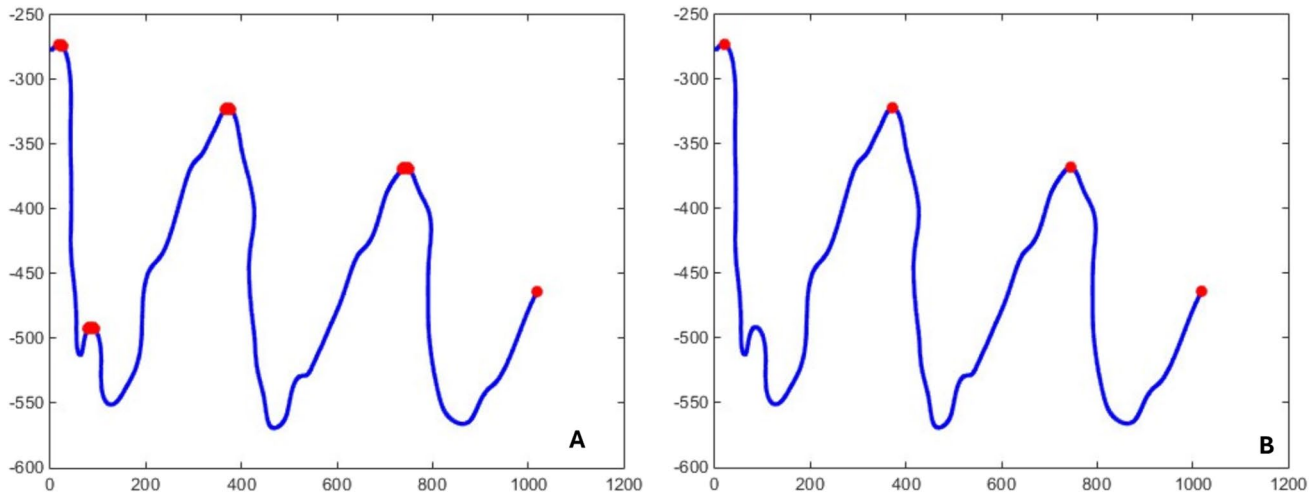

Fig. 4 **A** Peaks detected by neighbor analysis. **B** Peaks selected after filtering that excluded the false peaks

by different colors: white, purple, and black. We used the average of the image's RGB channels, μ_{RGB}, and the average of the difference between each pair of RGB channels, $diff_{RGB}$, to separate them: white elements are selected when we consider pixels with $\mu_{RGB} \geq 90$ and $diff_{RGB} < 30$; black elements are selected when we consider pixels with $\mu_{RGB} < 90$ and $diff_{RGB} < 30$; and purple elements are the remainder of non-selected pixels.

Pixels defining black elements (implant) are not used to compute the BIC and BBT, only white and purple elements, so the black elements are discarded. We counted the number of white and purple pixels inside BIC and BBT regions, respectively. These measurements are defined as the number of purple pixels divided by the (number of purple pixels + number of white pixels) inside a region. The machine used is equipped with Intel(R) Core (TM) i5-4440 CPU @ 3.10GHz, 16GB RAM, 64-bit Operating System and MATLAB R2018b 64-bit. The time required by the automated method to collect the %BIC and BBT data was measured.

Statistical Analysis

GraphPad Prism 9 software (San Diego, CA, USA) was utilized for inferential data analysis. As the data were normally distributed, indicated by the Shapiro–Wilk normality test, the Pearson's correlation test was employed to measure the degree of correlation between the %BIC and %BBT values from the two evaluation methods. A 95% confidence level was applied to all statistical tests used in this study.

Results

A high level of correlation was found between the manual and automated analyses of %BIC and %BBT ($r = 0.99$; $p < 0.001$). The time to perform all the measures by the automated method was around 30 s. Figures 7 A and B show the correlation graphs between the manual and automated evaluation methods for %BIC and %BBT, respectively.

Discussion

The time invested in the evaluation of histological images in scientific research, along with the need for team training, are some of the technical difficulties in histomorphometric analyses. Automated analysis methods have the potential to improve accuracy and reduce the afore mentioned technical difficulties, and the method proposed in the current study was shown to be reliable for assessing implant osseointegration through the analysis of %BIC and %BBT. In this first study, the script used is an initial version that meets only the specificities of this research. Based on the results presented, the script was useful for the evaluation of the osseointegration. However, some improvements may be permoed and tested to check if the good outcomes showed in this study may be maintained despite the variations of stain quality and methods.

Despite the convenience of data collection using the automation method, the process of creating the necessary script for its operation required time and study in the field of computing. The developed script uses a computer vision method based on the detection of color patterns through the RGB channels, allowing the computer to differentiate structures

Fig. 5 **A** Segmented image with ROI (region of interest) of the BIC. Red arrow, indicates the region of interest of BIC analysis. **B** Segmented image with ROI (region of interest) of the BBT. Black arrow, indicates the region of interest of BBT analysis

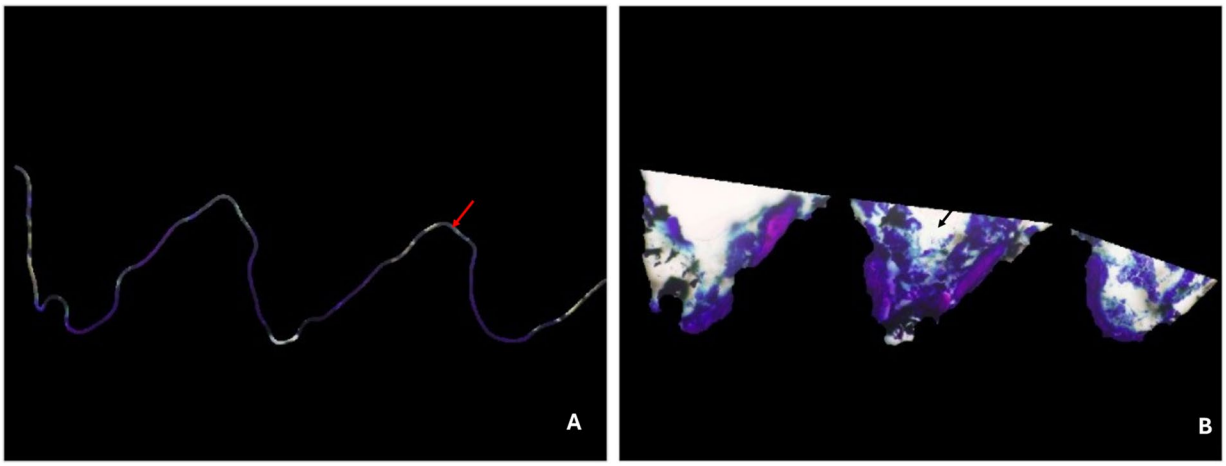

Fig. 6 **A** Image with ROI (region of interest) of the BIC without the segmentation filter. Red arrow, indicates the region of interest of BIC analysis. **B** Segmented image with ROI (region of interest) of the BBT without the segmentation filter. Black arrow, indicates the region of interest of BBT analysis

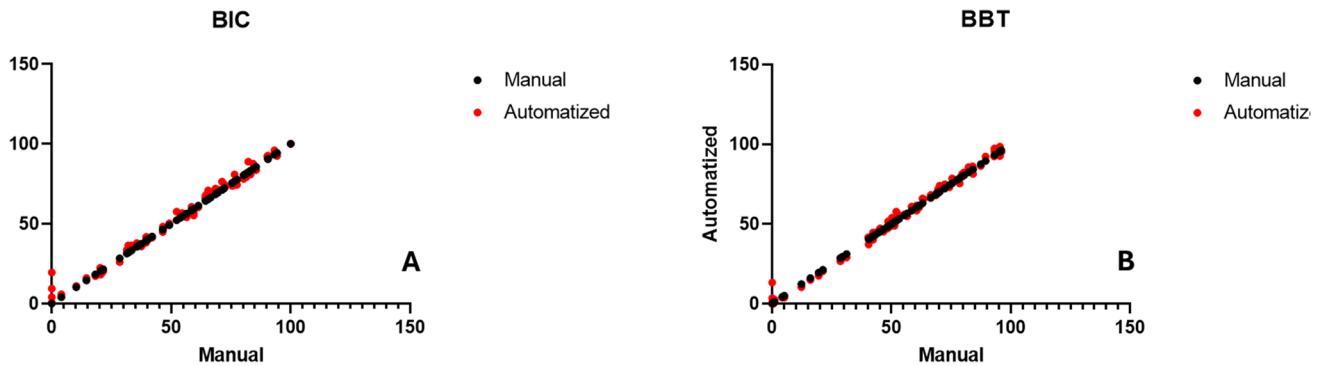

Fig. 7 Correlation graphs between the manual and automated evaluation methods of %BIC (**A**) and %BBT (**B**) respectively

based on the colors presented [13, 24–26]. For this automation process, some parameters used in several steps, such as segmentation, contour extraction, detection of the ROI, and the BIC and BBT had to be established through experimentation in order to deal with many variations present in the images (such as contrast and orientation) to finally obtain the analysis data.

In our study, the segmentation step was designed to separate the background (the black regions) from the foreground, which consists of the bone tissue and implant structures typically represented by white and purple tones in the images. Given that these regions are highly distinct in terms of intensity and color, the segmentation task does not present the typical challenges commonly addressed by advanced state-of-the-art segmentation methods. Techniques considered state-of-the-art (artificial intelligence techniques, such as convolutional neural networks) depend on a large amount of data to be used properly. Unfortunately, the limited number of samples in our study prevents many techniques from being properly used, as they could lead to biased results or overfitting. In addition, some combination of techniques are proposed to solve very specific problems. One example is the work [13]. Like ours, this work uses a combination of traditional image processing techniques to perform the segmentation of bone canals, a structure completely different from the one analyzed here, both in appearance and structure. As for the work [16], we can see that most of the techniques compared are traditional in literature, which demonstrates that they still play an important role in image processing in the most diverse fields of study. As shown by the results reported in the work [16], the K-means method, a traditional clustering algorithm, obtained the best accuracy in several databases, emphasizing the importance of these methods until nowadays.

Although it was not the objective of this study, the automated method turns the data collection process faster, as the %BIC and %BBT values from the 68 images analyzed were obtained within 30 s. Despite the time of evaluation by manual method was not measured, the reduction of the time of evaluation provided by the automated method was obviously. It is important to note that the data processing speed is directly related to the computational capacity of the machine used. In addition to the speed of data collection, automation can reduce the possibility of human errors, as manual analysis may be influenced by the evaluator's experience and training [27]. Therefore, research addressing implant osseointegration can provide faster and more accurate results, which could have a more immediate impact on the state of the art in rehabilitative treatment in dentistry and related fields.

Computational approaches have a wide range of applications in various areas of dentistry. Recent studies using an algorithm have shown good results in the detection of carious lesions through the analysis of periapical and interproximal radiographs [28, 29]. Other recent studies have evaluated the effectiveness of an algorithm for detecting sinusitis through the analysis of panoramic radiographs [30, 31]. A study by Nayak et al. (2006) [32] showed good results using artificial intelligence for the classification of pathological conditions by evaluating fluorescence spectroscopy in oral tissue. The findings of the current study and others [28–32] demonstrate that advances in computational areas for performing histological image analyses and other imaging exams present great potential to promote the replacement of manual analyses with automated methods.

The results obtained through automation in the current study are directly dependent on several factors, including the quality of the bone tissue staining. Since the entire data acquisition process relies on color pattern detection, poor staining quality of the histological slides can lead to false results or even prevent image analysis [20]. Although the conventional staining method currently has high predictability when performed by an experienced professional with appropriate equipment, there is still a possibility of errors in the process when these conditions are not met. A recent study, for example, compared the accuracy and precision of an experienced evaluator in detecting breast cancer in images with and without color correction treatment using artificial intelligence. In the untreated images, the accuracy and precision were 81.59% and 79.78%, respectively, while in images that underwent color correction treatment by the algorithm, the accuracy and precision increased to 92.87% and 92.33%, respectively [20]. In the present study, this type of correction was not necessary due to the uniform staining pattern of the slides used. In slides where this pattern is not achieved, it is possible that these adjustments would not reduce the accuracy of the automated evaluation; however, this hypothesis requires further testing.

Although the data acquisition method is automated, some processes still require human involvement to ensure that the results are as close to reality as possible. The presence of a human operator remains essential throughout the entire sample processing phase and during the pre-processing phase of the obtained images, guiding them spatially. The choice of parameters for the segmentation, contour extraction, ROI definition, BIC, and BBT calculations was defined by the operator. All parameters were established through extensive experimentation aimed at handling the considerable variability present in the images, such as differences in contrast, resolution, orientation, and anatomical features. For example, the choice of a radius like $r = 15$ was determined empirically by testing multiple values and observing their impact on the accuracy and consistency of the results across the dataset. The selected parameters represent a balance that ensures robust performance under the diverse conditions found in the images used. It is also worth noting that the script used

in this study was developed exclusively for the evaluation of osseointegrable implants in areas of native bone, and the staining method used was Stevenel's blue and acid fuchsine. For conditions different from those in the present study, adjustments need to be made to the script in order to avoid generating false results or preventing image analysis. Therefore, another limitation of this study is the fact that this is a first attempt to automate this analysis process, many adjustments will still need to be made in order to enable more generalist use of this resource by other researchers who use this analysis method.

Conclusion

The automated histomorphometric analysis method evaluated in the current study was shown to be reliable for obtaining BIC and BBT values of osseointegrated implants.

Author Contribution Lucas de Sousa Goulart Pereira, Guilherme José Lopes Pimentel de Oliveira, and André Ricardo Backes contributed to the study conception and design. Material preparation, data collection, and analysis were performed by Guilherme José Lopes Pimentel de Oliveira, Elcio Marcantonio Jr, André Ricardo Backes, and Jovânia Alves Oliveira. The first draft of the manuscript was written by Lucas de Sousa Goulart Pereira and all authors commented on previous versions of the manuscript. All authors read and approved the final manuscript.

Funding This study was financed by the Brazilian agencies CNPq (Conselho Nacional de Desenvolvimento Científico e Tecnológico, 426954/2018–1 and 307100/2021–9), CAPES (Coordenação de Aperfeiçoamento de Pessoal de Nível Superior–Brasil–Finance Code 001), and FAPEMIG (Fundação de Apoio a Pesquisa do Estado de Minas Gerais-APQ-02211–21).

Data Availability The data can be obtained upon request to the authors.

Declarations

Ethics Approval This study was performed in line with the ARRIVE principles. Approval was granted by process CEUA/FOAr #32/2016.

Competing interests The authors declare no competing interests.

References

1. Albrektsson T, Wennerberg A. On osseointegration in relation to implant surfaces. Clin Implant Dent Relat Res. 2019;21 Suppl 1:4-7. https://doi.org/10.1111/cid.12742. Epub 2019 Feb 28. PMID: 30816639.
2. Heydecke G, Boudrias P, Awad MA, De Albuquerque RF, Lund JP, Feine JS. Within-subject comparisons of maxillary fixed and removable implant prostheses: Patient satisfaction and choice of prosthesis. Clin Oral Implants Res. 2003 Feb;14(1):125-30. https://doi.org/10.1034/j.1600-0501.2003.140117.x. PMID: 12562375.
3. Trulsson U, Engstrand P, Berggren U, Nannmark U, Brånemark PI. Edentulousness and oral rehabilitation: experiences from the patients' perspective. Eur J Oral Sci. 2002 Dec;110(6):417-24. https://doi.org/10.1034/j.1600-0722.2002.21394.x. PMID: 12507214.
4. Pinotti FE, de Oliveira GJPL, Aroni MAT, Marcantonio RAC, Marcantonio E Jr. Analysis of osseointegration of implants with hydrophilic surfaces in grafted areas: A Preclinical study. Clin Oral Implants Res. 2018 Oct;29(10):963-972. https://doi.org/10.1111/clr.13361. Epub 2018 Sep 20. PMID: 30238514.
5. French D, Grandin HM, Ofec R. Retrospective cohort study of 4,591 dental implants: Analysis of risk indicators for bone loss and prevalence of peri-implant mucositis and peri-implantitis. J Periodontol. 2019 Jul; 90(7):691–700. doi: 10.1002/JPER.18-0236. Epub 2019 Feb 6. PMID: 30644101; PMCID: PMC6849729.
6. Oliveira VXR, Pinotti FE, Marcantonio RAC, Marcantonio E Jr, Oliveira GJPL. Comparison of osseointegration in areas grafted with different osteoconductive biomaterials. Preclinical study. Braz Dent J. 2022 Jan-Feb;33(1):105–111. doi: 10.1590/0103-6440202204378. PMID: 35262548; PMCID: PMC9645139.
7. Frisch E, Wild V, Ratka-Krüger P, Vach K, Sennhenn-Kirchner S. Long-term results of implants and implant-supported prostheses under systematic supportive implant therapy: A retrospective 25-year study. Clin Implant Dent Relat Res. 2020 Dec;22(6):689-696. https://doi.org/10.1111/cid.12944. Epub 2020 Sep 23. PMID: 32969180.
8. Schuster AJ, de Abreu JLB, Pola NM, Witek L, Coelho PG, Faot F. Histomorphometric analysis of implant osseointegration using hydrophilic implants in diabetic rats. Clin Oral Investig. 2021 Oct;25(10):5867-5878. https://doi.org/10.1007/s00784-021-03892-x. Epub 2021 Mar 25. PMID: 33765194.
9. Leocádio ACS, Júnior MS, Oliveira GJPL, Pinto GDCS, Faeda RS, Padovan LEM, Júnior ÉM. Evaluation of Implants with Different Macrostructures in Type I Bone-Pre-Clinical Study in Rabbits. Materials (Basel). 2020 Mar 26;13(7):1521. https://doi.org/10.3390/ma13071521. PMID: 32224982; PMCID: PMC7178163.
10. Spin-Neto R, Stavropoulos A, Coletti FL, Faeda RS, Pereira LA, Marcantonio E Jr. Graft incorporation and implant osseointegration following the use of autologous and fresh-frozen allogeneic block bone grafts for lateral ridge augmentation. Clin Oral Implants Res. 2014 Feb;25(2):226-33. https://doi.org/10.1111/clr.12107 . Epub 2013 Jan 25. PMID: 23346871.
11. Gonçalves VP, Pinotti FE, Spolidorio LC, Junior EM, de Oliveira GJPL, Steffens JP. Supraphysiologic Testosterone Administration Impairs Late Osseointegration in Male Rats. Int J Oral Maxillofac Implants. 2024 Feb 27;39(1):50-56. https://doi.org/10.11607/jomi.10263. PMID: 38416000.
12. Al Hezaimi K, Naghshbandi J, Nooh N, Schupbach P, Nevins M. Buccal Bone Remodeling Around Immediate Implants in STZ-Induced Diabetic Dogs: A Histologic and Microcomputed Tomographic Analysis. Int J Periodontics Restorative Dent. 2021 Sep-Oct;41(5):683–690. https://doi.org/10.11607/prd.4589. PMID: 34547070.
13. Gondim PHCC, Limirio PHJO, Rocha FS, Batista JD, Dechichi P, Travençolo BAN, Backes AR. Automatic Segmentation of Bone Canals in Histological Images. J Digit Imaging. 2021 Jun;34(3):678–690. https://doi.org/10.1007/s10278-021-00454-1. Epub 2021 May 4. PMID: 33948761; PMCID: PMC8329125.
14. Rodrigues LF, Backes AR, Travençolo BAN, de Oliveira GMB. Optimizing a Deep Residual Neural Network with Genetic Algorithm for Acute Lymphoblastic Leukemia Classification. J Digit Imaging. 2022 Jun; 35(3):623–637. doi: 10.1007/s10278-022-00600-3. Epub 2022 Feb 23. PMID: 35199257; PMCID: PMC9156643.
15. Hosseini MS, Bejnordi BE, Trinh VQ, Chan L, Hasan D, Li X, Yang S, Kim T, Zhang H, Wu T, Chinniah K, Maghsoudlou S,

Zhang R, Zhu J, Khaki S, Buin A, Chaji F, Salehi A, Nguyen BN, Samaras D, Plataniotis KN. Computational pathology: A survey review and the way forward. J Pathol Inform. 2024;15:100357. https://doi.org/10.1016/j.jpi.2023.100357. PMID: 38420608; PMCID: PMC10900832.
16. Andrade AR, Vogado LHS, Veras RMS, Silva RRV, Araujo FHD, Medeiros FNS. Recent computational methods for white blood cell nuclei segmentation: A comparative study. Comput Methods Programs Biomed. 2019 May;173:1-14. https://doi.org/10.1016/j.cmpb.2019.03.001. Epub 2019 Mar 6. PMID: 31046984.
17. Garcia-Lamont F, Lopez-Chau A, Cervantes J, Ruiz S. Nucleus segmentation of white blood cells in blood smear images by modeling the pixels' intensities as a set of three Gaussian distributions. Med Biol Eng Comput. 2024;62(8):2371-2388. https://doi.org/10.1007/s11517-024-03065-4. Epub 2024 Apr 8. PMID: 38584206.
18. Martos O, Hoque MZ, Keskinarkaus A, Kemi N, Näpänkangas J, Eskuri M, Pohjanen VM, Kauppila JH, Seppänen T. Optimized detection and segmentation of nuclei in gastric cancer images using stain normalization and blurred artifact removal. Pathol Res Pract. 2023 Aug;248:154694. https://doi.org/10.1016/j.prp.2023.154694. Epub 2023 Jul 16. PMID: 37494804.
19. Altini N, Marvulli TM, Zito FA, Caputo M, Tommasi S, Azzariti A, Brunetti A, Prencipe B, Mattioli E, De Summa S, Bevilacqua V. The role of unpaired image-to-image translation for stain color normalization in colorectal cancer histology classification. Comput Methods Programs Biomed. 2023 Jun;234:107511. https://doi.org/10.1016/j.cmpb.2023.107511. Epub 2023 Mar 26. PMID: 37011426.
20. Salvi M, Michielli N, Molinari F. Stain Color Adaptive Normalization (SCAN) algorithm: Separation and standardization of histological stains in digital pathology. Comput Methods Programs Biomed. 2020 Sep;193:105506. https://doi.org/10.1016/j.cmpb.2020.105506. Epub 2020 Apr 17. PMID: 32353672.
21. Patil S, Albogami S, Hosmani J, Mujoo S, Kamil MA, Mansour MA, Abdul HN, Bhandi S, Ahmed SSSJ. Artificial Intelligence in the Diagnosis of Oral Diseases: Applications and Pitfalls. Diagnostics (Basel). 2022 Apr 19;12(5):1029. https://doi.org/10.3390/diagnostics12051029. PMID: 35626185; PMCID: PMC9139975.
22. Ilhan B, Lin K, Guneri P, Wilder-Smith P. Improving Oral Cancer Outcomes with Imaging and Artificial Intelligence. J Dent Res. 2020;99(3):241-248. https://doi.org/10.1177/0022034520902128. PMID: 32077795; PMCID: PMC7036512.
23. Backes, A. R., Travençolo, B. A. N., & Escarpinati, M. C. A derivative based algorithm for image thresholding. In Proceedings of the XII Workshop of Computational Vision (pp. 189–194), 2016.
24. Gonzalez, R. C., & Woods, R. E. . Digital Image Processing. Pearson; 3ª edição, 2000.
25. Dougherty, E. R. Digital image processing methods. CRC Press, 2020.
26. de Andrade, R.G., Durval, M.C., Ferreira, I.M. et al. Automated assessment of water holding capacity in digital images. SIViP 16, 465–472 (2022).
27. Irie MS, Spin-Neto R, Teixeira LHS, Rabelo GD, Reis NTA, Soares PBF. Effect of micro-CT acquisition parameters and individual analysis on the assessment of bone repair. Braz Oral Res. 2023 Oct 27;37:e099. https://doi.org/10.1590/1807-3107bor-2023.vol37.0099. PMID: 38055517.
28. Lee JH, Kim DH, Jeong SN, Choi SH. Detection and diagnosis of dental caries using a deep learning-based convolutional neural network algorithm. J Dent. 2018 Oct;77:106-111. https://doi.org/10.1016/j.jdent.2018.07.015. Epub 2018 Jul 26. PMID: 30056118.
29. Cantu AG, Gehrung S, Krois J, Chaurasia A, Rossi JG, Gaudin R, Elhennawy K, Schwendicke F. Detecting caries lesions of different radiographic extension on bitewings using deep learning. J Dent. 2020;100:103425. https://doi.org/10.1016/j.jdent.2020.103425 .Epub 2020 Jul 4. PMID: 32634466.
30. Kuwana R, Ariji Y, Fukuda M, Kise Y, Nozawa M, Kuwada C, Muramatsu C, Katsumata A, Fujita H, Ariji E. Performance of deep learning object detection technology in the detection and diagnosis of maxillary sinus lesions on panoramic radiographs. Dentomaxillofac Radiol. 2021;50(1):20200171. https://doi.org/10.1259/dmfr.20200171.
31. Kim Y, Lee KJ, Sunwoo L, Choi D, Nam CM, Cho J, Kim J, Bae YJ, Yoo RE, Choi BS, Jung C, Kim JH. Deep Learning in Diagnosis of Maxillary Sinusitis Using Conventional Radiography. Invest Radiol. 2019 Jan;54(1):7-15. https://doi.org/10.1097/RLI.0000000000000503. PMID: 30067607.
32. Nayak GS, Kamath S, Pai KM, Sarkar A, Ray S, Kurien J, D'Almeida L, Krishnanand BR, Santhosh C, Kartha VB, Mahato KK. Principal component analysis and artificial neural network analysis of oral tissue fluorescence spectra: classification of normal premalignant and malignant pathological conditions. Biopolymers. 2006;82(2):152-66. https://doi.org/10.1002/bip.20473. PMID: 16470821.